SEGMENTATION OF VESSEL GEOMETRIES FROM MEDICAL IMAGES USING GPF DEFORMABLE MODEL

Si Yong Yeo[1], Xianghua Xie[2], Igor Sazonov[1] and Perumal Nithiarasu[1]

[1]*College of Engineering, Swansea University, Swansea , U.K.*
[2]*College of Science, Swansea University, Swansea , U.K.*

Keywords: Vessel segmentation, Geometric potential force, Deformable model, Image segmentation, Level set methods.

Abstract: We present a method for the reconstruction of vascular geometries from medical images. Image denoising is performed using vessel enhancing diffusion, which can smooth out image noise and enhance vessel structures. The Canny edge detection technique which produces object edges with single pixel width is used for accurate detection of the lumen boundaries. The image gradients are then used to compute the geometric potential field which gives a global representation of the geometric configuration. The deformable model uses a regional constraint to suppress calcified regions for accurate segmentation of the vessel geometries. The proposed framework show high accuracy when applied to the segmentation of the carotid arteries from CT images.

1 INTRODUCTION

The human circulatory system consists of vessels that transport blood throughout the body, providing the tissues with oxygen and nutrients. It is known that vascular diseases such as stenosis and aneurysms are often associated with changes in blood flow patterns and the distribution of wall shear stress. Modelling and analysis of the hemodynamics in the human vascular system can improve our understanding of vascular disease, and provide valuable insights which can help in the development of efficient treatment methods. In recent years, computational fluid dynamics (CFD) has been widely used for patient-specific modelling of blood flow in vascular structures (Steinman, 2002; Cebral et al., 2003; Taylor and Figueroa, 2009; Taylor and Steinman, 2010). Despite the involvement of numerous groups working in this field, and rapid advancement in efficient computational methods, there has been limited applications of computational hemodynamics in clinical practice. This is largely due to the challenges involved in the design of an integrated framework which can efficiently and accurately automate the interdisciplinary computational modelling process, which includes image segmentation, mesh generation and CFD simulation.

One of the main challenges in the computational modelling of hemodynamics is the accurate reconstruction of the vascular geometry. Anatomically accurate geometric models of the vascular structures are essential for realistic flow simulations and analysis. The anatomical information used to reconstruct the geometric models are usually provided in the form of medical image datasets (scans) from imaging modalities such as computed tomography (CT) and magnetic resonance (MR) imaging. Manual reconstruction of the vasculature geometries can be tedious and time consuming. There is also the issue of variability between the geometries extracted manually by different individuals, and variability of geometries extracted by the same individual at different occasions. In order to allow computational flow modelling to be efficiently applied as a diagnostic or predictive tool, the amount of user intervention required in the process should be reasonably small. In particular, a considerable amount of user intervention is often required in the reconstruction of an accurate geometric model for the simulation of flow dynamics. Therefore a robust and efficient method that can be used to accurately segment the geometric structures from medical image datasets can be very useful and advantageous in the modelling process. Here, we propose a robust framework for the segmentation of vessel geometries using the GPF deformable model. The framework is then applied to efficiently segment the geometries of carotid arteries from CT images.

Although several techniques exist for the segmentation of vascular structures from medical images, it remains an intricate process due to factors such as image noise, partial volume effects, image artifacts, in-

tensity inhomogeneity and changes in topology. In (Mori and Yamaguchi, 2001), the coordinate points for the center line of the aortic arch were extracted from volume rendered MR images. A cubic spline was then used to represent the aortic centerline, and cross-sectional grids were generated on normal planes at equidistant points along the curve. This generated a curved tube with circular cross section of uniform radius, which is not representative of the geometry of the aorta. In (Tokuda et al., 2008), the centerline and diameter information of the vessels was extracted from the image dataset, and the vascular model was reconstructed using non-uniform rational B-splines (NURBS). Such techniques may often smooth out geometric information that can be important to the computation of accurate flow dynamics, such as those at bifurcations.

The 3D models of the vascular structures in (Wang et al., 1999) were reconstructed by extracting the 2D contours of the vessels at each of the image slices of the MR image dataset, and then lofting through the contours to create the surface models of the vessels. The different vessels were then merged using boolean operations in solid modelling. The cross sections of a particular vessel may however intersect with cross sections of branching vessels, and the geometry at these positions have to be approximated. Other authors such as (Xu et al., 1999; Augst et al., 2003; Younis et al., 2004; Giordana et al., 2005; Peiro et al., 2008) also reconstructed 3D surface models of the vessels from 2D contours extracted from image slices. This sometimes requires positioning and orienting the 2D contours according to the medial axis of the vessels, and curve and surface interpolation are used to approximate and reconstruct the surface models. However, the 2D contour extraction techniques used do not provide control over 3D smoothness, and 3D geometric properties from the image datasets are not considered.

A simple thresholding technique was used in (Nanduri et al., 2009) to extract the binary image of the vessels, and the vascular model was reconstructed using an isosurface algorithm. The thresholding technique however does not consider the spatial characteristics of the image, and is sensitive to image noise and inhomogeneous intensity. In (Yi and Ra, 2003; Sekiguchi et al., 2005), region growing algorithms were applied to segment the vascular structures from CT and MR angiography data. The region growing techniques are, in general, sensitive to noise, and can often lead to non-contiguous regions and over-segmentation. In addition, thin structures are often not extracted due to variations in image intensities. The watershed transform was used in (Abdel-Dayem

and El-Sakka, 2005; Ding et al., 2007) to extract the geometry of the carotid. In this approach, the image is interpreted as a landscape or topographic surface, with the pixel intensity representing the elevation of the topographic surface. Consider water on the landscape flowing towards regions with local minima, the watersheds are the lines that partition these regions. In this way, the image is partitioned into homogeneous regions with the watersheds defining the boundaries of the regions. The watershed transform tends to be sensitive to noise and often produces over-segmentation. It is also difficult for the watershed technique to extract thin structures and weak object edges.

In (Ladak et al., 2000; Gil et al., 2000), a 3D dynamic surface model was used to delineate the boundary of carotid arteries. An initial triangulated model was placed within the interior of the carotid vessels, and an inflation force was applied to deform the model towards the vessel wall. In particular, the inflation force is applied only when the vertices of the model are within the lumen, i.e., at locations with image intensity below a user-specified threshold. An image-based force is further applied to the surface model to better localize the boundary. It may however be difficult to select an appropriate threshold value that delineates the vessel wall closely due to inhomogeneous image intensity. This approach is sensitive to noise, and manual editing is often required to move the vertices towards the vessel wall. In (Steinman et al., 2002), a 2D discrete dynamic contour was first used to extract the vessel contours, a dynamic surface model was then inflated to reconstruct the surface model using the binary images of the extracted contours. This however does not consider the 3D geometric information from the image dataset. In (Yim et al., 2001; Cebral et al., 2001; Cebral et al., 2004), the surface models for each of the vessel branches of the carotid artery were reconstructed independently using a tubular deformable model. A surface merging algorithm is then required to reconstruct the surface model of the carotid bifurcation from the triangulated surfaces of the vessel branches. This particular approach requires the determination of the axis of each of the vessels, which can be done manually by selecting a reasonable amount of points from image slices to represent the curves of the structure. Due to the smoothing effect of this technique, regions of high curvature such as those at bifurcations or stenosis may not be modeled accurately. These explicit deformable models represent contours and surfaces parametrically, which requires the tracking of points on the curves and surfaces during deformation. It is therefore difficult for explicit deformable models to

deal with topological variation and complex shapes.

Implicit deformable models have been applied in the segmentation of vascular structures in (Nilsson and Heyden, 2003; Antiga and Ene-Iordache, 2003; Deschamps et al., 2004; Svensson et al., 2006; Antiga et al., 2008). However, many of these techniques use an attraction force field which acts on contours or surfaces only when they are close to the object boundaries. As such, initial contours have to be placed close to the object boundaries, which can be tedious in complex geometries. A constant pressure term such as the one in (Malladi et al., 1995), is often used to monotically expand or shrink the deformable model towards the image object boundaries, which can overwhelm weak object edges. In addition, the initial contours have to be placed either inside or outside object boundaries, which can be difficult for compact and narrow structures. Many of these techniques are also sensitive to image noise, and have difficulties in extracting deep boundary concavities.

2 PROPOSED METHOD

In this section, a robust framework is proposed for the reconstruction of vascular geometries from medical images. The approach consists of image denoising using vessel enhancing diffusion (Enquobahrie et al., 2007; Manniesing et al., 2006), optimal edge detection using the Canny edge filter (Canny, 1986), and robust segmentation of the vascular geometries using GPF deformable model (Yeo et al., 2011).

2.1 Vessel Enhancing Diffusion Filtering

The formulation of the vessel enhancing diffusion filter (Enquobahrie et al., 2007; Manniesing et al., 2006) is based on a smoothed version of the vesselness measure used in (Frangi et al., 1998). In this approach, an anisotropic diffusion filter with strength and direction determined by the vesselness measure is applied to enhance the geometric structures of the vessel. The vesselness measure is determined by analyzing the eigensystem of the Hessian matrix given as:

$$\mathbf{H} = \begin{bmatrix} I_{xx} & I_{xy} & I_{xz} \\ I_{yx} & I_{yy} & I_{yz} \\ I_{zx} & I_{zy} & I_{zz} \end{bmatrix} \quad (1)$$

which describes the geometric information at each point of a 3D image I based on the local intensity variations. Here, the derivatives of the image I are computed as convolution with derivatives of the Gaussian function, i.e. $I_x = I(\mathbf{x}) * \frac{\partial}{\partial x} G_\sigma(\mathbf{x})$, where G_σ denotes the Gaussian function with standard deviation σ. The

principal curvatures and directions are given by the maximum and minimum eigenvalues and the corresponding eigenvectors. With the eigenvalues given such that $|\lambda_1| \leq |\lambda_2| \leq |\lambda_3|$, the vesselness measure is defined as: if $\lambda_2 \geq 0$ or $\lambda_3 \geq 0$, $V_\sigma(\lambda) = 0$; otherwise

$$V_\sigma(\lambda) = \left(1 - e^{\frac{-R_A^2}{2\alpha^2}}\right) \cdot e^{\frac{-R_B^2}{2\beta^2}} \cdot \left(1 - e^{\frac{-S^2}{2\gamma^2}}\right) \cdot e^{\frac{2c^2}{|\lambda_2||\lambda_3|^2}} \quad (2)$$

with

$$R_A = \frac{|\lambda_2|}{|\lambda_3|} \quad (3)$$

$$R_B = \frac{|\lambda_1|}{\sqrt{|\lambda_2 \lambda_3|}} \quad (4)$$

$$S = \sqrt{\lambda_1^2 + \lambda_2^2 + \lambda_3^2} \quad (5)$$

in which R_A and R_B can be used to differentiate tubular structures from blob-like and plate-like structures, while S is used to differentiate between foreground vessel structures and background noise. The parameters α, β and γ are weighting factors which control the sensitivity of the vesselness measure, and c is a small constant.

For a multiscale analysis, the vesselness function is computed for a range of scales, and the maximum response is selected using the following equation:

$$V = \max_{\sigma_{min} \leq \sigma \leq \sigma_{max}} V_\sigma(\lambda) \quad (6)$$

A diffusion tensor is then defined such that vessel diffusion takes place in the direction of the vessel, while diffusion perpendicular to the vessel direction is inhibited. The diffusion tensor can therefore be used to preserve vessel structures and is given as:

$$\mathbf{D} = \mathbf{Q}\lambda'\mathbf{Q}^T \quad (7)$$

where $\mathbf{Q}$ is a matrix containing the eigenvectors of the Hessian matrix $\mathbf{H}$, and λ' is a diagonal matrix with elements given as:

$$\lambda_1' = 1 + (w - 1) \cdot V^{\frac{1}{s}} \quad (8)$$

$$\lambda_2' = \lambda_3' = 1 + (\varepsilon - 1) \cdot V^{\frac{1}{s}} \quad (9)$$

with w, ε and s as tuning parameters. The anisotropic diffusion is then defined as:

$$L_t = \nabla \cdot (\mathbf{D}\nabla L) \quad (10)$$

where $L(0)$ is set as the input image. Figure 1 demonstrates that the vessel enhancing diffusion filter can be applied to enhance the vessel structures and smooth out noise in the image. The algorithm for the vessel enhancing diffusion filter has been implemented using the Insight Toolkit (Ibanez et al., 2005).
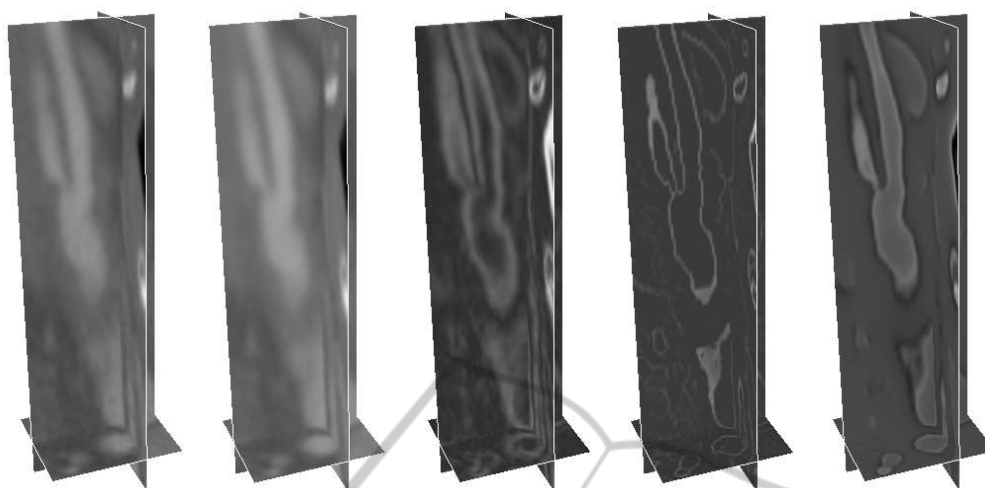
Figure 1: Vessel enhancing diffusion and image object edge representation of CT image dataset 1, from left to right - original image, image with vessel enhancing diffusion, image gradient magnitude, Canny edge with image gradient intensities, geometric potential field.

2.2 Edge Representation for Vessel Geometries

Image object edges are usually represented as regions with high intensity contrasts. Image gradients can be determined using the gradient operator or the Sobel filter. These techniques however produces object edge width of a few pixels. This can easily cause nearby structures to be connected. For complex geometries such as those in medical images, it is often necessary to determine fine edges using more robust edge detection techniques (Deriche, 1987; Petrou and Kittler, 1991) for accurate representation of the image structures. The Canny edge detection (Canny, 1986) can produce object edges with single pixel width, and can therefore be used for accurate edge detection of the vessel structures. In the Canny edge detection technique, image smoothing is first applied to reduce noise interference. This can be performed using the Gaussian filter or other smoothing techniques such as vessel enhancing diffusion (Manniesing et al., 2006). The image gradients are then computed to determine the magnitudes and directions of the edges. Image pixels with magnitudes which are not local maxima in the directions of the edges are suppressed. Hysterisis thresholding is then applied to filter out spurious edges caused by noise. Image pixels with edge magnitude greater than a high threshold, i.e. $f_{edge}(x) > T_h$ are considered as edges, while pixels with edge magnitude lower than a low threshold, i.e. $f_{edge}(x) < T_l$ are removed. Image pixels with edge magnitudes in between the threshold values, i.e. $T_l \leq f_{edge}(x) < T_h$, which are connected to edge pixels are also considered as edges. The image gradients at the detected edges are then used to compute the geometric potential field, see (Yeo et al., 2011) for more detail. As shown in Figure 1, the geometric potential field gives a more coherent representation of the image object boundaries as it utlizes global edge pixel interactions across the image.

2.3 Segmentation of Vessel Geometries using GPF Deformable Model with Region Constraint

It is shown in (Yeo et al., 2009a; Yeo et al., 2009b; Yeo et al., 2011) that the GPF deformable model can be used to efficiently segment complex geometries from biomedical images. By using pixel or voxel interactions across the whole image domain, the deformable model is more robust to image noise and weak edges. The dynamic vector force field changes according to the relative postition and orientation between the geometries, which allows the deformable model to propagate through long tubular structures.

Here, the GPF deformable model is applied to segment the geometries of human carotid arteries from CT images. Some of the main challenges in the segmentation of the carotid geometries include intensity inhomgeneity, weak edges and adjacent veins with similar intensities to the carotids. In addition, calcifications which are attached to the arterial walls should not be included in the reconstructed geometries. Although, the calcified plaques often appear as relatively bright regions compared to soft tissues, plaques with lower densities may have similar intensities to the lumen. As the intensities of the plaques vary with the
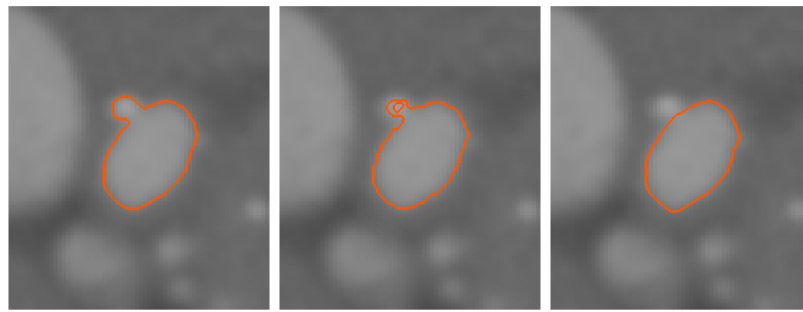
Figure 2: Image slice from CT image dataset 2 showing contours (top row) and corresponding pixels (bottom row) extracted using: from left to right - GPF deformable model, GPF deformable model with intensity threshold and GPF deformable model with region constraint.

Figure 3: Image slice from CT image dataset 4 showing contours (top row) and corresponding pixels (bottom row) extracted using: from left to right - GPF deformable model, GPF deformable model with intensity threshold and GPF deformable model with region constraint.

densities, it is not easy for techniques such as global intensity threshold to remove the plaques from the extracted geometries. In this section, a region constraint is added to the deformable model such that it does not propagate across the calcified regions. This is done by constraining the deformable model from propagating across regions with image gradient magnitude larger than a user specified value, T_{max}. As the calcified regions usually have relatively large image gradients, the threshold value can be easily selected by observing the histogram of the image gradient magnitude. The deformable model with region constraint can thus be expressed as:

$$\frac{\partial \phi}{\partial t} = \begin{cases} 0 & \text{if } |\nabla I| > T_{max} \\ \alpha g \kappa |\nabla \phi| - (1-\alpha)(\mathbf{F} \cdot \nabla \phi) & \text{otherwise} \end{cases}$$

(11)

where α is a weighting parameter, g is the edge stopping function, κ is the curvature and $\mathbf{F}$ is the geometric potential force defined in the GPF model (Yeo et al., 2011).

Figures 2 and 3 depict a z-axis slice of the extracted geometry. As shown in the figures, some calcified regions have similar intensity to the lumen, which caused the deformable model to include them in the extracted geometries. The intensities of the plaques vary which makes it difficult for a global intensity threshold to suppress them. It is shown that by adding the region constraint, the deformable model can easily get around the calcified regions to segment the carotid geometries accurately.

3 RESULTS AND DISCUSSION

In this section, experimental results on the segmentation of the cartoid geometries using the proposed framework are shown. In particular, 6 datasets from CT imaging (provided by Wolverhampton NHS trust) are used in the experiment. The volumes of interest containing the carotid arteries are extracted from the image datasets to reduce the size of the input datasets. The robust framework which consits of vessel diffusion enhancing, computation of optimal object edge representation and deformable model with regional constraint is then applied for the reconstruction of vessel geometries.

Figures 4 to 7 depict the segmentation of the carotid geometries using the GPF deformable model with region constraint. As shown in Figures 4 and 6, the bidirectional and dynamic vector force allows the flexible cross-boundary intializations of the model to easily propagate and converge to the geometries of the
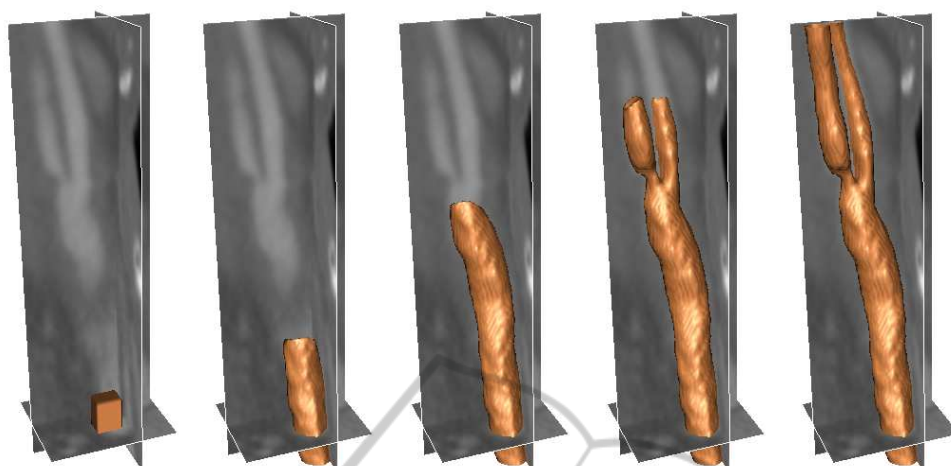
Figure 4: Segmentation of carotid artery from CT image dataset 1 (61x71x125) using GPF deformable model (CPU-time, 276s).
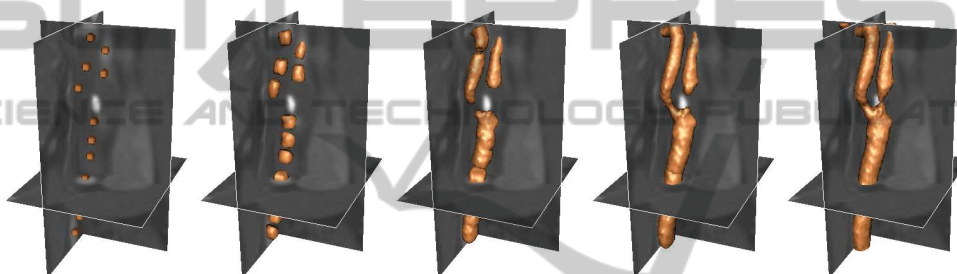

Figure 5: Segmentation of carotid artery from CT image dataset 3 (70x80x120) using GPF deformable model (CPU-time, 206s).
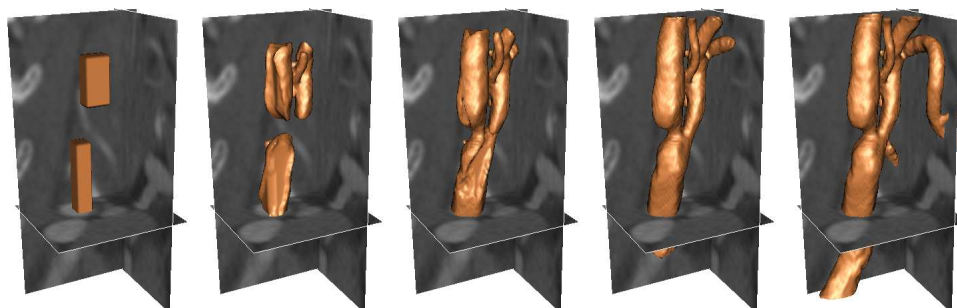

Figure 6: Segmentation of carotid artery from CT image dataset 5 (70x80x120) using GPF deformable model (CPU-time, 1379s).
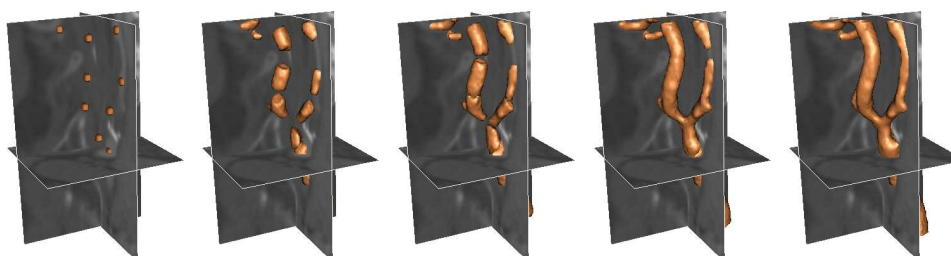

Figure 7: Segmentation of carotid artery from CT image dataset 6 (70x80x120) using GPF deformable model (CPU-time, 185s).
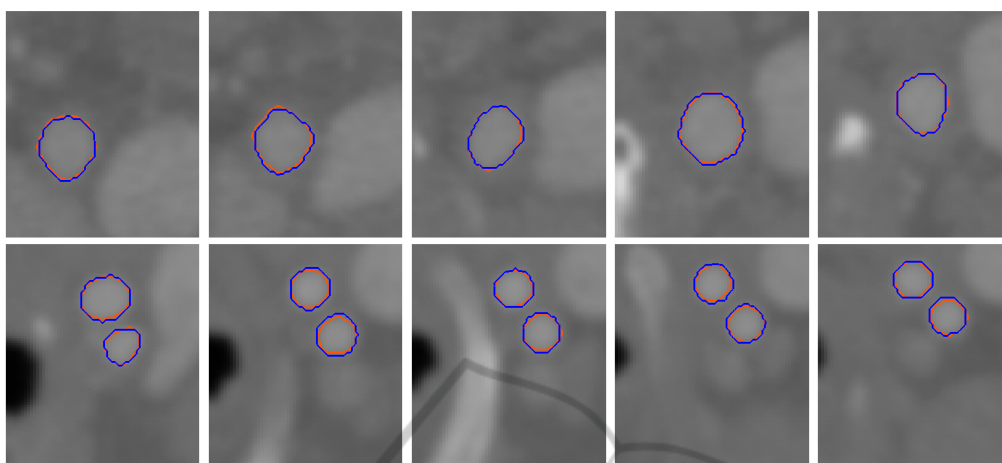
Figure 8: Comparison of geometry segmented from CT image dataset 1 using image slices taken along z-axis direction: blue - manual, orange - GPF deformable model.
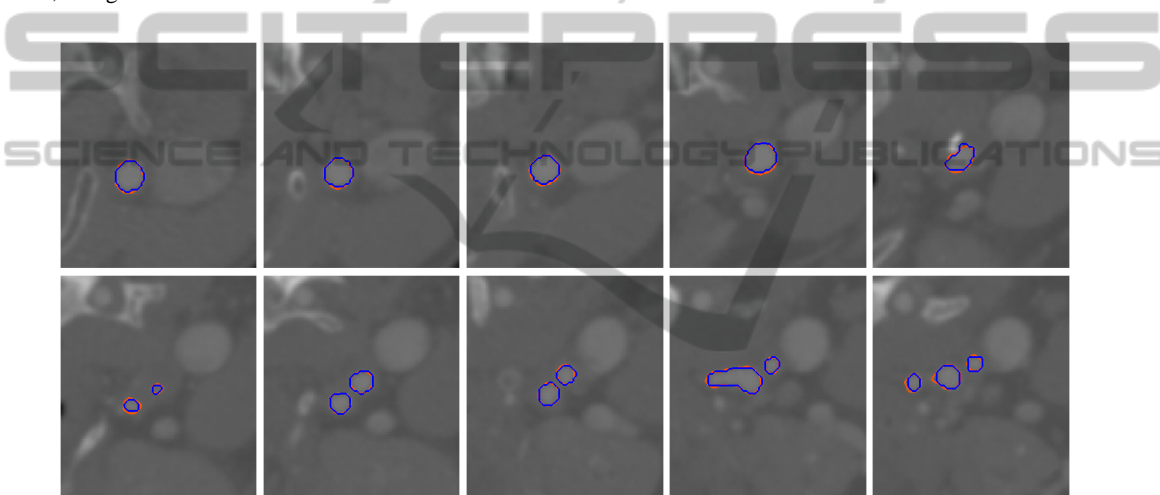

Figure 9: Comparison of geometry segmented from CT image dataset 3 using image slices taken along z-axis direction: blue - manual, orange - GPF deformable model.

carotid arteries. The extraction of the vessel geometries from image datasets 1 and 4 took only 276s and 494s, while the extraction from image datasets 2 and 5 took 1216s and 1379s due to factors such as intensity variation, low constrast, multiple branches and complex topologies. A graphical user interface has been developed, which can be used to set multiple initial contours for fast convergence. It can also be used to remove inconsistency in object boundaries due to low resolution of the images, artifacts, etc., or small branches which do not affect the computational flow analysis. As shown in Figure 5 and Figure 7, one can easily speed up the segmentation process by placing multiple initial contours or surfaces, as the model converges to the vessel geometries in 206s and 185s when applied to image datasets 3 and 6 respectively. Note that the deformable model easily propagate through the stenotic carotid bifurcations and get around the

calcified regions to efficiently segment the carotid geometries from the CT images.

The reconstructed vessel geometries using the proposed framework are compared against geometries from manual segmentation. Figures 8 to 11 depict the comparison of the extracted geometries using random cross-section slices taken along the z-axis direction. The blue and orange contours represent the cross-section of the geometries extracted manually and using the GPF deformable model respectively. As shown in the figures, the image dataset consist of other tissue structures which may affect the geometric reconstruction. In particular, vessels adjacent to the carotid artery can often cause other models to leak out due to the similar intensity. The geometric potential field provides a more coherent and global representation of the object edges, and allows the deformable model to extract the geometry accu-
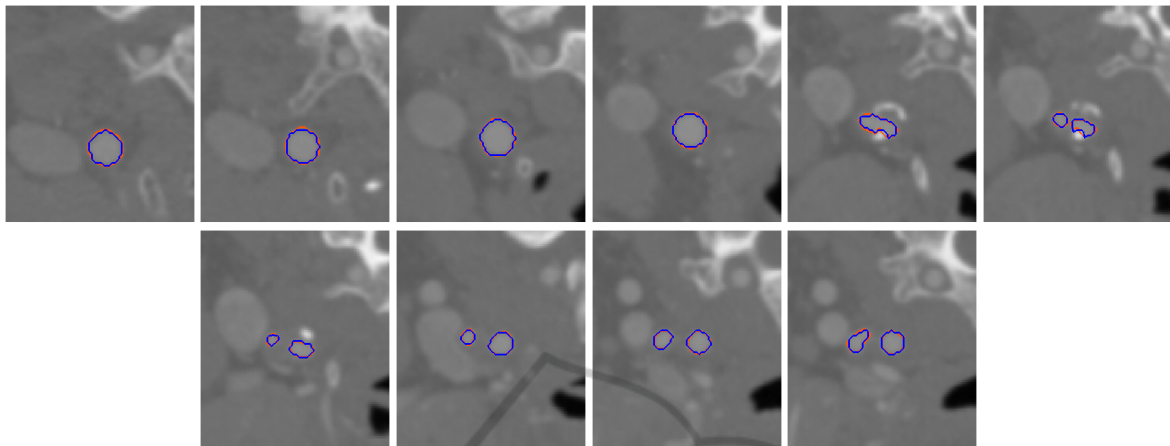
329

Figure 10: Comparison of geometry segmented from CT image dataset 4 using image slices taken along z-axis direction: blue - manual, orange - GPF deformable model.

Figure 11: Comparison of geometry segmented from CT image dataset 6 using image slices taken along z-axis direction: blue - manual, orange - GPF deformable model.

rately. By adding a region constraint, the proposed model can easily get around the calcified regions as the deformable model propagates through the tubular structures to segment the vessel geometry as depicted in Figures 9, 10 and 11. The proposed framework can therefore be applied to segment the vessel geometries efficiently from the images. As shown in the figures, the vessel geometries segmented using the GPF deformable model with region constraint exhibit considerably small deviations from the manually extracted geometries.

Table 1 presents the accuracy of the segmented geometries using the proposed method. The foreground (FG) and background (BG) accuracy of the geometries were measured as the percentages of true foreground and background voxels which were segmented as foreground and background respectively. The normalized overall accuracy is given as the average of FG and BG to measure the accuracy of cor-

Table 1: Comparison of the segmented carotid geometries using the GPF deformable model with manual segmentation: Foreground (FG), background (BG) and overall accuracy measured in %.

CT image dataset	GPF	
1	FG (%)	89.9
	BG (%)	99.9
	Overall (%)	**94.9**
2	FG (%)	89.8
	BG (%)	99.9
	Overall (%)	**94.8**
3	FG (%)	96.0
	BG (%)	99.9
	Overall (%)	**97.9**
4	FG (%)	99.1
	BG (%)	99.8
	Overall (%)	**99.5**
5	FG (%)	93.8
	BG (%)	99.5
	Overall (%)	**96.7**
6	FG (%)	94.4
	BG (%)	99.6
	Overall (%)	**97.0**
FG Average (%)		**93.9**
BG Average (%)		**99.8**
Overall Average (%)		**96.8**

rectly extracted voxels to reduce measurement bias towards the large number of background voxels in the image. It is shown that the proposed framework provides significantly accurate geometries with overall acurracies of 94.9%, 94.8%, 97.9%, 99.5%, 96.7% and 97.0% for image datasets 1 to 6, and an average overall accuracy of 96.8%.

REFERENCES

Abdel-Dayem, A. and El-Sakka, M. (2005). Carotid artery ultrasound image segmentation using fuzzy region growing. In *International Conference on Image Analysis and Recognition*, pages 869–878.

Antiga, L. and Ene-Iordache, B. Remuzzi, A. (2003). Computational geometry for patient-specific reconstruction and meshing of blood vessels from mr and ct angiography. *IEEE T-MI*, 22(5):674–684.

Antiga, L., Piccinelli, M., Botti, L., Ene-Iordache, B., Remuzzi, A., and A., S. D. (2008). An image-based modeling framework for patient-specific computational hemodynamics. *Medical and Biological Engineering and Computing*, 46(11):1097–1112.

Augst, A. D., Barratt, D. C., Hughes, A. D., McG Thom, S. A., and Xy, X. Y. (2003). Various issues relating to computational fluid dynamics simulations of carotid bifurcation flow based on models reconstructed from three-dimensional ultrasound images. *Proc Inst Mech Eng H, Journal of Engineering in Medicine*, 217(5):393–403.

Canny, J. (1986). A computational approach to edge detection. *IEEE T-PAMI*, 8(6):679–698.

Cebral, J. R., Castro, M. A., Lohner, R., Burgess, J. E., Pergolizzi, R., and Putman, C. M. (2004). Recent developments in patient-specific image-based modeling of hemodynamics. In *ENIEF04*.

Cebral, J. R., Hernandez, M., and Frangi, A. F. (2003). Computational analysis of blood flow dynamics in cerebral aneurysms from cta and 3d rotational angiography image data. In *International Congress on Computational Bioengineering*, pages 191–198.

Cebral, J. R., Lohner, R., Soto, O., Choyke, P. L., and Yim, P. J. (2001). Patient-specific simulation of carotid artery stenting using computational fluid dynamics. In *MICCAI*, pages 153–160.

Deriche, R. (1987). Using canny's criteria to derive a recursively implemented optimal edge detector. *IJCV*, 1(2):167–187.

Deschamps, T., Schwartz, P., Trebotich, D., Colella, P., Saloner, D., and Malladi, R. (2004). Vessel segmentation and blood flow simulation using level-sets and embedded boundary methods. In *Computer Assisted Radiology and Surgery*, pages 75–80.

Ding, S., Tu, J., Cheung, C., Beare, R., Phan, T., Reutens, D., and Thien, F. (2007). Geometric model generation for CFD simulation of blood and air flows. In *International Conference on Bioinformatics and Biomedical Engineering*, pages 1335–1338.

Enquobahrie, A., Ibanez, L., Bullitt, E., and Aylward, S. (2007). Vessel enhancing diffusion filter. *The Insight Journal*.

Frangi, A. F., Niessen, W. J., Vincken, K. L., and Viergever, M. A. (1998). Multiscale vessel enhancement filtering. In *MICCAI*, pages 130–137.

Gil, J. D., Ladak, H. M., Steinman, D. A., and Frenster, A. (2000). Accuracy and variability assessment of a semiautomatic technique for segmentation of the carotid arteries from three-dimensional ultrasound images. *Medical Physics*, 27(6):1333–1342.

Giordana, S., Sherwin, S. J., Peiro, J., Doorly, D. J., Papaharilaou, Y., Caro, C. G., Watkins, N., Cheshire, N., Jackson, M., Bicknall, C., and Zervas, V. (2005). Automated classification of peripheral distal by-pass geometries reconstructed from medical data. *Journal of Biomechanics*, 38(1):47–62.

Ibanez, L., Schroeder, W., Ng, L., and Cates, J. (2005). *The ITK Software Guide, 2nd Edition*. Kitware, Inc.

Ladak, H. M., Milner, J. S., and Steinman, D. A. (2000). Rapid three-dimensional segmentation of the carotid bifurcation from serial MR images. *Journal of Biomechanical Engineering*, 122(1):96–99.

Malladi, R., Sethian, J. A., and Vemuri, B. C. (1995). Shape modelling with front propagation: A level set approach. *IEEE T-PAMI*, 17(2):158–175.

Manniesing, R., Viergever, M. A., and Niessen, W. J. (2006). Vessel enhancing diffusion: A scale space representation of vessel structures. *Medical Image Analysis*, 10(6):815–825.

Mori, D. and Yamaguchi, T. (2001). Construction of the CFD model of the aortic arch based on mr images and simulation of the blood flow. In *International Workshop on Medical Imaging and Augmented Reality*, pages 111–116.

Nanduri, J. R., Pino-Romainville, F. A., and Celik, I. (2009). CFD mesh generation for biological flows: Geometry reconstruction using diagnostic images. *Computers & Fluids*, 38(5):1026–1032.

Nilsson, B. and Heyden, A. (2003). A fast algorithm for level set-like active contours. *Pattern Recognition Letters*, 24(9):1311–1337.

Peiro, J., Sherwin, S. J., and Giordana, S. (2008). Automatic reconstruction of a patient-specific high-order surface representation and its application to mesh generation for CFD calculations. *Medical and Biological Engineering and Computing*, 46(11):1069–1083.

Petrou, M. and Kittler, J. (1991). Optimal edge detectors for ramp edges. *IEEE T-PAMI*, 13(5):483–491.

Sekiguchi, H., Sugimoto, N., Eiho, S., Hanakawa, T., and Urayama, S. (2005). Blood vessel segmentation for head MRA using branch-based region growing. *Systems and Computers in Japan*, 36(5):80–88.

Steinman, D. A. (2002). Image-based computational fluid dynamics modeling in realistic arterial geometries. *Annals of Biomedical Engineering*, 30(4):483–497.

Steinman, D. A., Thomas, J. B., Ladak, H. M., Milner, J. S., Rutt, B. K., and Spence, J. D. (2002). Reconstruction of carotid bifurcation hemodynamics and wall thickness using computational fluid dynamics and mri. *Magnetic Resonance in Medicine*, 47(1):149–159.

Svensson, J., Gardhagen, R., Heiberg, E., Ebbers, T., Loyd, D., Lanne, T., and Karlsson, M. (2006). Feasibility of patient specific aortic blood flow CFD simulation. In *MICCAI*, pages 257–263.

Taylor, C. A. and Figueroa, C. A. (2009). Patient-specific modeling of cardiovascular mechanics. *Annual Review of Biomedical Engineering*, 11:109–134.

Taylor, C. A. and Steinman, D. A. (2010). Image-based modeling of blood flow and vessel wall dynamics: Applications, methods and future directions. *Annals of Biomedical Engineering*.

Tokuda, Y., Song, M.-H., Ueda, Y., Usui, A., Toshiaki, A., Yoneyama, S., and Maruyama, S. (2008). Three-dimensional numerical simulation of blood flow in the aortic arch during cardiopulmonary bypass. *European Journal of Cardio-thoracic Surgery*, 33(2):164–167.

Wang, K. C., Dutton, R. W., and Taylor, C. A. (1999). Improving geometric model construction for blood flow modeling. *IEEE Engineering in Medicine and Biology Magazine*, 18(6):33–39.

Xu, X. Y., Long, Q., Collins, M. W., Bourne, M., and Griffith, T. M. (1999). Reconstruction of blood flow patterns in human arteries. *Proc Inst Mech Eng H, Journal of Engineering in Medicine*, 213(5):411–421.

Yeo, S. Y., Xie, X., Sazonov, I., and Nithiarasu, P. (2009a). Geometric potential force for the deformable model. In *BMVC*.

Yeo, S. Y., Xie, X., Sazonov, I., and Nithiarasu, P. (2009b). Level set based automatic segmentation of human aorta. In *International Conference on Computational and Mathematical Biomedical Engineering*.

Yeo, S. Y., Xie, X., Sazonov, I., and Nithiarasu, P. (2011). Geometrically induced force interaction for three-dimensional deformable models. *IEEE T-IP*, 20(5):1373–1387.

Yi, J. and Ra, J. B. (2003). A locally adaptive region growing algorithm for vascular segmentation. *International Journal of Imaging Systems and Technology*, 13(4):208–214.

Yim, P. J., Cebral, J. J., Mullick, R., Marcos, H. B., and Choyke, R. L. (2001). Vessel surface reconstruction with a tubular deformable model. *IEEE T-MI*, 20(12):1411–1421.

Younis, H. F., Kaazempur-Mofrad, M. R., Chan, R. C., Isasi, A. G., Hinton, D. P., Chau, A. H., Kim, L. A., and Kamm, R. D. (2004). Hemodynamics and wall mechanics in human carotid bifurcation and its consequences for atherogenesis: investigation of inter-individual variation. *Biomechanics and Modeling in Mechanobiology*, 3(1):17–32.